Cooperative Behavior in Driven Lattice Systems with Shifted Periodic Boundary Conditions

Mark J. Anderson

Dissertation submitted to the Faculty of the Virginia Polytechnic Institute and State University in partial fulfillment of the requirements for the degree of

DOCTOR OF PHILOSOPHY
in
PHYSICS

APPROVED:

R.K.P. Zia, Chairman
J.R. Heflin
B. Schmittmann
C. D. Williams
D. A. deWolf

April 17, 1998
Blacksburg, Virginia

Keywords: Monte-Carlo Simulations, Lattice Gas, Non-equilibrium steady states

Cooperative Behavior in Driven Lattice Systems with Shifted Periodic Boundary Conditions

Mark J. Anderson

(ABSTRACT)

We explore the nature of driven stochastic lattice systems with non-periodic boundary conditions. The systems consist of particle and holes which move by exchanges of nearest neighbor particle-hole pairs. These exchanges are controlled by the energetics associated with an internal Hamiltonian, an external drive and a stochastic coupling to a heat reservoir. The effect of the drive is to bias particle-hole exchanges along the field in such a way that a particle current can be established. Hard-core volume constraints limit the occupation of only one particle (hole) per lattice site. For certain regimes of the overall particle density and temperature, a system displays a homogeneous disordered phase. We investigate cooperative behavior in this phase by using two-point spatial correlation functions and structure factors. By varying the particle density and the temperature, the system orders into a phase separated state, consisting of particle-rich and particle-poor regions. The temperature and density for the co-existence state depend on the boundary conditions. By using Monte Carlo simulations, we establish co-existence curves for systems with shifted periodic boundary conditions.

To Linda, Matthew, Scott,
my mother and father

Contents

Acknowledgements **iii**

1 INTRODUCTION **1**

2 THE LATTICE GAS, IN AND FAR FROM EQUILIBRIUM **5**
2.1 The equilibrium Ising lattice gas 5
2.2 The Katz-Lebowitz-Spohn lattice gas 7
2.3 The KLS model with shifted periodic boundary conditions 9

3 TWO-PARTICLE CORRELATIONS IN THE DISORDERED PHASE **13**
3.1 Microscopics of the Simulations and Typical Configurations 13
3.2 Two-point Correlations in Systems with PBC and SPBC 15
3.3 Ordinary and Skewed Structure Factors 23

4 Densities of co-existing phases in half-filled systems **34**
4.1 Methodologies 35
4.2 Typical configurations in a "heating-cooling" cycle 37
4.3 Cluster sizes, cluster densities, and the co-existence curve 42

5 Order-disorder transitions: phase diagram in the $\bar{\rho}$-T plane **46**
5.1 Order Parameters 46
5.1.1 Structure Factors 47
5.1.2 Column densities and fluctuations 47
5.1.3 Cluster sizes and densities 51
5.1.4 Internal energy 51
5.1.5 Co-existence curves 52
5.2 Two systems with PBC (H=0) 52
5.2.1 Systems with varying $\bar{\rho}$ and the coexistence curve for $H = 0$. 62
5.3 Systems with SPBC 63
5.3.1 Two Systems with SPBC(H=3) 64

5.3.2 Two Systems with SPBC (H=4) 65
5.3.3 Two Systems with SPBC (H=9) 69
5.3.4 Two Systems with SPBC (H=18) 71
5.3.5 Systems with varying $\bar{\rho}$ 73
5.3.6 Co-existence Curves 75

6 Co-existence of a System with Large Fluctuations 77
6.1 Method I 77
6.2 Method II 79
6.3 Metastable States 87

7 Summary and Outlook 92
7.1 Summary 92
7.2 Outlook 95

Appendix A: Definition of $\tilde{G}$ at integer values 97

Appendix B: Skewed symmetry of $e^{i\tilde{\mathbf{k}}\cdot\mathbf{x}}$ 98

Appendix C: Example of S and $\tilde{S}$ for different ordered states 99

Appendix D: Cluster Distributions and Configurations 102

Vita 112

Acknowledgments

I thank my Ph.D. advisor Prof. Royce Zia for his steadfast guidance and effort in supporting this dissertation. I deeply appreciate his encouragement and teaching throughout the years. I also thank Prof. Beate Schmittmann for her encouraging conversations. Both of them have made this study into non-equilibrium systems both a challenge and a joy.

I thank my employer, NSWCDD for supporting this effort financially. In particular, I thank Dr. Thomas Clare for supporting long term training and John Hagy for coordinating the training. I thank my management, Dr. David Lando, John Harvey and Jane Robinson for their constant support.

I thank Mike Rudzinsky for his software support and helpful conversations. I also deeply appreciate the many encouraging conversations I had with Jim Maroney over the years. He has patiently taught me many computer programming skills. These skills have greatly helped me perform the numerous Monte Carlo studies in an efficient, repeatable and systematic fashion. I thank Dr. Zoltan Toroczkai for helping me organize this dissertation into its final form.

I thank Chris Thomas and the other Physics Department's secretaries for their assistance. I thank Denise Wise, my branch secretary, for her countless submissions of training proposals.

I thank my mother, father, siblings, in-laws, relatives and friends for their enthusiastic support. Finally, I thank my wife Linda and my two sons, Matthew and Scott, for their love, patience and sacrifice.

1. INTRODUCTION

A century ago, Boltzmann and Gibbs laid the foundations for statistical mechanics of systems in equilibrium with a thermal bath at temperature T [1]. In that formulation, the energy, or Hamiltonian $H[C]$, associated with each configuration C of the system plays a central role, through the expression

$$P_{eq}[C] \propto \exp\left(-H[C]/k_B T\right) \tag{1.1}$$

which states that the probability for finding the system in C is proportional to the Boltzmann factor and k_B is the Boltzmann constant. All macroscopic properties of the system can be determined as statistical averages over all configurations, weighted by (1.1). However, most systems in nature are not in equilibrium. To describe these statistically would require, in general, a time dependent probability $P[C,t]$. Further progress typically relies on deriving, or postulating, a differential equation for this quantity. A widely used case is the Master equation, on which this thesis is based. If our system were coupled to a single reservoir of energy (a thermal bath), this equation should lead us, as $t \to \infty$, to the stationary solution: $P^*[C] = P_{eq}$. If, on the other hand, our system is coupled to more than one reservoir (e.g., two baths at different temperatures), then we should expect $P^*[C] \neq P_{eq}$ in general. In particular, there would be a constant flux of energy *through our system*, even though all probabilities are time-independent. Very little is known about such *non-equilibrium steady state* systems, especially if they are not "near" equilibrium states (e.g., two baths at infinitesimally distinct T's). Recently, a simple model of such a many-body system was proposed: the driven Ising lattice gas [2]. Indeed, it displays many surprising phenomena, by contrast to the well known equilibrium case. Since its introduction, considerable progress toward its understanding was made, though many aspects remain puzzling [3]. This study is devoted to the effects of non-periodic boundary conditions on this simple, yet rich, model of non-equilibrium steady states.

The driven lattice gas was partly motivated by the physics of fast ionic conductors [4]. In these conductors, large ions (e.g., silver) hop from site to site on an underlying crystalline lattice, responding to both the thermal environment and external applied electric fields. Generally, it is highly unlikely that two ions can

occupy the same site, so that this system is well modeled by the lattice gas version of the Ising model [5, 6]. Furthermore, due to Coulombic and elastic forces, the ions interact in a non-trivial way. In most cases, the effective interaction is short ranged and may be attractive or repulsive, to be modelled by nearest neighbor interactions in the Ising model. Thus, a configuration of the model is specified by the occupation numbers $\{n_\sigma\}$, where $n_\sigma = 0$ or 1 represents an empty or occupied site σ in, say, a (two-dimensional, $d = 2$) square lattice. The Hamiltonian is just

$$\mathcal{H}[\{n_\sigma\}] = -J \sum n_\sigma n_{\sigma'} \tag{1.2}$$

with σ, σ' being nearest neighbor sites and J (> 0 or < 0) representing the strength of the (attractive or repulsive) interaction. For simplicity, periodic boundary conditions (PBC) are typically imposed, so that the system is translational invariant. In the absence of external fields, most of the *equilibrium* thermodynamic properties are well known [7, 6, 8]. In particular, for a system with fixed particle (ion) density ($\rho \equiv \sum n_i/V$) and $J > 0$, the high temperature phase is disordered and the density is homogeneous. In this dissertation, $V = LM$ where L and M are the two dimensions of our lattice. At sufficiently low temperatures, the system displays two co-existing phases, one particle-rich (density ρ_+) and the other particle-poor (density ρ_-). The analytic derivation of the coexistence curve, $\rho_\pm(T)$, for the $d = 2$ Ising model is an important milestone in the history of statistical mechanics [7, 9]. The next major triumph is surely the renormalization group [10], which, through the ideas of universality, allows us to conclude that critical behavior of a class of complex, real systems are identical to those in the simple Ising model.

To describe evolution and properties away from equilibrium, the Ising model must be endowed with some form of dynamics. The two most common forms are non-conserved [11] and conserved dynamics [12], the former being more appropriate for application of the Ising model to spin system. In the latter, the total particle number is conserved ($\sum n_\sigma$=constant), more appropriate for ions. Thus, we will restrict our considerations to only models with conserved dynamics. Here, the particles hop from site to site, governed by rates which simulate the coupling to a *single* heat bath. Unlike the equilibrium Ising model, much less is known about the dynamic properties analytically.

Applying an external electric field corresponds to coupling our system to *two* energy reservoirs, so that the dynamics must be modified. In 1984 [2], Katz, Lebowitz and Spohn (KLS) introduced an utterly simple modification to the above model: biasing the hopping rates for jumps in the field direction. When this system reaches steady state, there would be a constant (particle) current, while P^* is definitely not P_{eq}. Phenomena, totally unexpected under equilibrium

conditions, were discovered mainly through Monte Carlo simulations. For example, while the second order phase transition (for the $d = 2$ system) survives, long range correlations and singular structure factors are present at *all temperatures* above criticality. Below the transition temperature, T_c, co-existence is displayed, though only in the form of strips *parallel* to the drive (inhomogeneity transverse to the field). More unexpected phenomena appeared, again with the help of computer simulations. In 1987 Marro and Valles concluded that there are *two* coexistence curves [6]. So far, no other systematic study has been undertaken to confirm these conclusions.

Meanwhile, the interface between the co-existing phases is found to be "smooth" or faceted [13], rather than diverging with system size, as in equilibrium. Following equilibrium ideas that facets are intimately related to singularities of the interface energy (as a function of the interface orientation) [14], Valles, Leung and Zia [15] performed simulations of this driven Ising lattice gas with *shifted periodic boundary conditions* (SPBC). Another term being "screw periodicity", these conditions imply that a particle leaving the "bottom edge" will return at a *shifted* location on the "top edge." (Periodic BC is retained on the right/left edges. Figure 1.1)

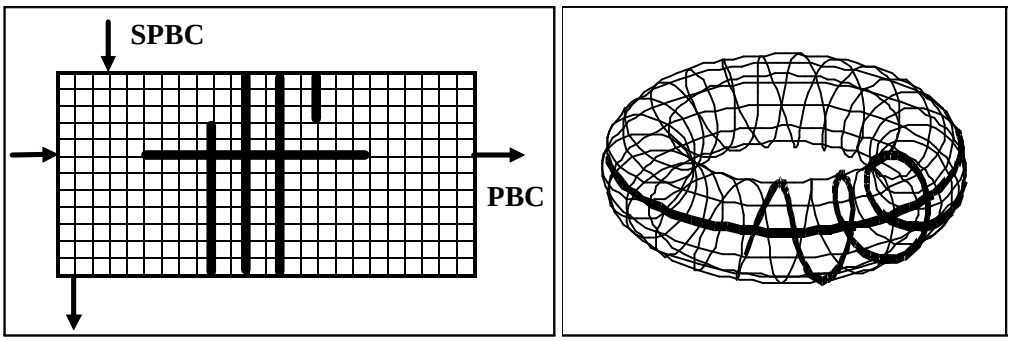

Figure 1.1 A Lattice with SPBC and the Toroidal Representation

Using SPBC is the standard method for inducing interfaces at different orientations for phase separated systems. Surprisingly, there are singularities in the *bulk* energy, resulting in *multistrip* phases being more stable at high shifts. As a result of these new phases, the notion of a unique co-existence curve requires further clarification. Since this study was performed only on half-filled systems, a systematic investigation at various densities should shed light on these issues. In this sense, this dissertation generalizes and synthesizes the studies of Marro,

et. al. [16, 17]and Valles, et. al.[15], through simulations of a driven Ising lattice gas with SPBC, in a range of shifts and densities.

Most of the study focuses on a system of 72×36, so that many commensurate shifts can be implemented. For low shifts, the system still orders into a single, but "tilted", strip at low temperatures, so that the co-existence curves can be mapped out. For high shifts, the system always orders into "multistrip phases." A variety of methods are introduced to delineate where the transition occurs. Within statistical errors and finite size rounding, all give consistent results. In addition, the two-point correlation function and structure factors have been studied in some of the systems.

This dissertation is organized as follows.

In Chapter 2, the details of the model, as well as a brief review of previous studies, are presented. How the simulations are performed, as well as investigations of two-point correlations and structure factors, are discussed in Chapter 3. In Chapter 4, we estimated the co-existence curves by studying the behavior of half-filled systems. The co-existence curves are established by a different methodology in Chapter 5. Here, we study co-existence by using a variety of order parameters. While Chapters 4 and 5 are devoted to the results for relatively well behaved SPBC systems, Chapter 6 discusses the extraordinary fluctuations in a critical system. Chapter 7 summarizes the dissertation and provides an outlook for future studies.

2. THE LATTICE GAS, IN AND FAR FROM EQUILIBRIUM

In this chapter, we present our model in detail, starting with the lattice gas in equilibrium (2.1) and in various non-equilibrium settings (2.2).

2.1. The equilibrium Ising lattice gas

The model of our focus is a generalized Ising lattice gas [5, 6] in $d = 2$. On a square lattice with PBC, the sites are labelled by (i, j) with $i \in [1, L]$ and $j \in [1, M]$, so that the occupation numbers are $\{n(i, j)\}$. Given the Hamiltonian (1.2), the equilibrium properties, in the thermodynamic limit, are well known [7, 8]. In particular, there is a second order phase transition for a half-filled system at the Onsager temperature $0.5673J/k_B$. In the rest of this thesis, this quantity will be used as *the unit* of T, the temperature. Above $T = 1$, the system is disordered with a homogeneous (average) density given by the fixed overall density ρ. Below that, the system displays *phase co-existence,* provided

$$\rho_-(T) < \rho < \rho_+(T) \quad . \tag{2.1}$$

A connected region of low density (ρ_-) will co-exist with a particle-rich one (density ρ_+), with appropriate areas to satisfy the overall density of ρ. Thus, $\rho_\pm(T)$ is known as the (two branches of the) co-existence curve.

It is often convenient to use the spin language of the Ising lattice gas. At each site, the spin variable s can take values $+1$ or -1. Identifying these with the site being occupied or empty, we see that

$$s = 2n - 1.$$

In this language, the particle-hole symmetry in $\mathcal{H}$ is manifest in its invariance under the global change: $s \to -s$. As a result, $\rho_\pm(T) = [1 \pm m(T)]/2$, where $m(T)$ is known as the spontaneous magnetization. The exact co-existence curve for the lattice gas $\rho_\pm(T)$ comes from the celebrated analytic form of $m(T)$ [7, 9].

Clearly, if the overall density ρ is very close to either ρ_+ or ρ_-, the connected region of the opposite phase will gather into a droplet with a single domain boundary. As ρ is changed towards $1/2$ (with fixed T), the size of this droplet will be larger, until some critical value is reached[18] when the domain will encircle the torus across the shorter dimension, i.e., $\min(L, M)$. Two domain boundaries (interfaces) appear, both *necessarily* aligned with the lattice orientation. Various properties of these interfaces, e.g., profiles and widths, are known and can be compared to simulation results. Interfaces with other orientations can only be accessed by imposing *SPBC*, as detailed below. It is clear that, to minimize interface energy, the domain will still encircle the torus in the "shortest" way possible, even though the interfaces are no longer aligned with the lattice (Figure 2.1).

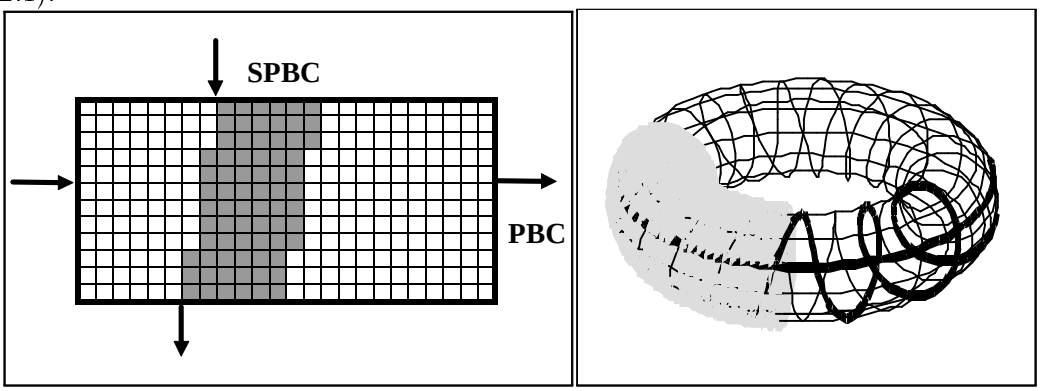

Figure 2.1 A Domain of the Ising model on a Lattice with SPBC and the Toroidal Representation

Since we will be interested in non-equilibrium properties, we must specify its dynamics as well, i.e., an equation for its time evolution. For this we rely on the Master equation for the probability to find the system in configuration C at time t: $P[C,t]$. Letting $W[C \to C']$ denote the transition rate from C to C', this equation reads

$$\partial_t P[C,t] = \sum_{C'} \left(W[C' \to C] P[C',t] - W[C \to C'] P[C,t] \right) \quad . \tag{2.2}$$

This equation can be used to describe systems evolving towards the equilibrium state, provided the rates satisfy certain constraints. In that case, to ensure

that any initial distribution $P[C,0]$ will settle, as $t \to \infty$, into the equilibrium $P_{eq}[C]$ (1.1), all we need is that W is a function of

$$\beta\Delta\mathcal{H} = \beta\left(\mathcal{H}[C'] - \mathcal{H}[C]\right)$$

alone, obeying the detailed balance condition:

$$W(\xi)/W(-\xi) = e^{-\xi} \quad . \tag{2.3}$$

While it is not necessary to keep this condition for arbitrary non-equilibrium systems, we will be interested in those which can be tuned, continuously, to the equilibrium case. Thus, in all our models, rates obey "local detailed balance," as will be seen below.

For us, another important constraint is particle conservation, so that the dynamics can involve only "particle-hole exchanges". To simulate real particle diffusion, we simply allow only exchanges of a *nearest neighbor pair*, i.e., Δi or Δj being ± 1 (mod L or M, respectively). Clearly, these exchanges can be thought of as particle hops to an unoccupied neighboring site. In Monte Carlo simulations, the most favorite is the Metropolis rate [20]:

$$W[C \to C'] = \min\{1, \exp(-\beta\Delta\mathcal{H})\} \tag{2.4}$$

where C and C' differ only by a nearest neighbor particle-hole pair.

2.2. The Katz-Lebowitz-Spohn lattice gas

Motivated by the physics of fast ionic conductors [4] and the quest for new behavior in non-equilibrium steady states, Katz, Lebowitz and Spohn [2] introduced a seemingly "harmless" modification to the above model, by applying a local DC drive to the particles. To be precise, we imagine the particles being "charged" and imposing an "electric" field E. Except for the PBC, such a drive can be incorporated into $\mathcal{H}$ by adding the term

$$\sum_{i,j} jEn(i,j) \tag{2.5}$$

which favors/suppresses hops along/against a "downwards" pointing field (Figure 2.1) Indeed, this also describes particles in a constant gravitational field. *However*, imposing PBC is incompatible with (2.5), which spoils translational invariance. Nevertheless, it is possible to define a translationally invariant *rate* which models such a drive:

$$W[C \to C'] = \min\{1, \exp(-\beta\Delta\mathcal{H} + E\Delta j)\} \quad . \tag{2.6}$$

Note that Δj must be computed modulo M to account for the PBC. While this is still ± 1 for jumps from/to $j = 1, M$, a similar trick fails in (2.5) as j mod M suffers a discontinuity at one row of the torus. As a result, the steady state distribution P^* is not given simply by $Z^{-1} \exp\left[-\beta\left(\mathcal{H} + \sum_{i,j} jEn(i,j)\right)\right]$. More importantly, unlike P^*_{eq}, it does not satisfy global detail balance relation. For equilibrium, we have

$$W[C \to C']P^*_{eq}[C] = W[C' \to C]P^*_{eq}[C'].$$

For non-equilibrium, we have

$$W[C \to C']P^*[C] \neq W[C' \to C]P^*[C']$$

for all pairs $\{C, C'\}$. Since the difference of these two sides is a measure of the net steady state probability current between C and C', we could make an analogy to electromagnetism here. While equilibrium states are analogues of electrostatics, with time independent charge distribution and *zero* current, these states correspond to those in magnetostatics with a time independent charge distribution and a *non-zero* steady current.

For very small systems (up to 2x4), the Master equation (2.2) with (2.6) can be solved exactly to give P^* [21, 22]. Though these studies reveal interesting and important differences between equilibrium and non-equilibrium steady state properties, they shed very little light on co-operative phenomena in the thermodynamic limit. Instead, such properties comes mainly from Monte Carlo simulation studies and continuum field theoretic analysis[3].

From simulations, this non-equilibrium system is found to display a second order transition at all E, with $T_c(E) > 1$ and $\rho = 1/2$. Above criticality, the two point correlation function displays power law decay[23], as opposed to exponential decay in equilibrium. Correspondingly, the structure factor is singular at the origin [24], unlike the Ornstein-Zernike form in the $E = 0$ case. The critical properties, predicted from renormalization group analysis [25], fall outside the universality class of the equilibrium Ising model [10]. Subsequent simulations with finite size scaling analysis largely confirm these results[26]. Below criticality, the system displays phase co-existence, though only strips *parallel* to the drive (i.e., inhomogeneity *transverse* to E) are seen. Simulating with half-filled systems with $E = \infty$, Marro and Valles [16] measured the densities of these phases and reported the co-existing curve $\rho_\pm(T)$. Incidentally, we should mention that, using systems with *off-critical* densities, these authors found first order transitions *within* the $\rho_\pm(T)$ above, leading them to conclude that there are *two* co-existence curves [16]! However, these measurements have not been independently verified. Nor

has there been a systematic study of finite size effects, which would, naively, lead to similar conclusions for equilibrium systems.

2.3. The KLS model with shifted periodic boundary conditions

Though they seem to be academic, shifted periodic boundary conditions provide indispensable tools to investigate the properties of interfaces between co-existence phases. With PBC alone, the interfaces will always be aligned, on the average, with one of the lattice axes. To induce interfaces with other orientations, SPBC must be imposed. This "trick" is exploited extensively for equilibrium Ising models [27], in both $d = 2$ and 3, for finding orientation dependence of interfacial energies, the relationship to the statistical width of interfaces and the roughening transition [28]. Typically, in only one direction is the boundary condition shifted. For the $d = 2$ model specifically, this implies the site $(i, 1)$ is a nearest neighbor to $(i + H, M)$ for all i (and, of course, similarly for $(1, j)$ and (L, j)). In particular, when a particle at $(i, 1)$ is driven "downwards", it reappears at $(i + H, M)$. We will refer to H as *the shift.*

Naturally, similar questions about the properties of interfaces in a *driven system* arose. In contrast to the undriven system, in which the interfacial width diverges with the square root of the linear system size, the effect of the drive is found to "smooth out" the interface [13] so that the width appears to converge. In this sense, E affects the interface like a gravitational field, suppressing all fluctuations above the capillary height. Subsequently, a more detailed investigation found the height-height correlations to be singular in the small wave-vector limit [29]. For equilibrium systems, there is a well known connection between smooth interfaces (facets) and kinks in the interfacial energy as a function of the orientation [14]. Exploring the possibility that this connection survives in the driven case, Monte Carlo simulations with *SPBC* were carried out [15], so that energies associated with interfaces at various orientations can be measured. Here, "energy" simply refers to the average value of $\mathcal{H}$ which is directly related to the number of particle-particle pairs. Much to the surprise of these authors, there is a kink singularity associated with the *bulk energy*! In sharp contrast, SPBC does not affect *bulk* quantities in equilibrium. This behavior can be explained qualitatively by noting that the two interfaces in a tilted strip are not equivalent, since the drive breaks particle-hole symmetry. The interface with the particle-rich phase "upstream" will act as a source of particles for the hole-rich bulk, since there is a component of E across the interface, stripping particles from the dense phase. Similarly, holes will be stripped and sent in the opposite direction. As a result, this interface is more diffusive and is referred to as the "evaporating edge".

On the other hand, an interface with the particle-rich phase "downstream" acts more as a sink for particle-hole pairs, since both particle and hole are driven into this region. This denser region will be called the "absorbing edge".

Even more remarkable is that, for larger and larger shifts, the system undergoes a series of novel transitions, as a result of the competition between the drive and the interparticle attraction. First, there is a "splitting" transition, where the simple phase separated state with a single (dense) strip transforms into one with multiple strips. While J favors a single "tilted" strip (so as to minimize surface energy), E tries to align the interfaces "vertically" (parallel to the drive). For large H, the drive wins and, by taking the form of a single, thinner strip with multiple winding around the torus (Figure 2.1), the interfaces can be much better aligned with E. If the shift is commensurate with L, the system may display L/H *vertical* strips. Otherwise, the multiple strips will also be tilted, though not as much as in the single strip case. As H increases further, the tilt of this multi-strip phase will increase. As a result, there follows a sequence of "merging" transitions, where an n-strip state becomes an $(n-1)$-strip state. Though the mechanism of these new transitions is qualitatively understood, a quantitatively reliable theory remains elusive [30].

Since the main motivation of the studies using SPBC lies in interfacial properties, the Monte Carlo simulations were performed only for half-filled, $L = M$ systems at $T = 0.8$. In this study, we focus on the *bulk* properties of a driven system with SPBC, such as two-point correlation functions in the disordered phase and the co-existence curve in the low temperature phase. The model is the same as that described in the previous two sections. To keep the study manageable, we kept the size fixed, at $L = 72$, $M = 36$, and explored the three-dimensional parameter space (H, ρ, T) of shift, overall density, and temperature. The choice of 72×36 is obviously motivated by the many divisors available.

Before discussing the Monte Carlo investigations, we present the exact results for P^* in a small system, 2×3. Though these will not give us much information concerning phase transitions, they will offer some interesting contrast to the ones for the driven PBC case. Following [21, 22], we group the total of 20 configurations into 4, based on symmetry of translational invariance alone. (Figure 2.2) Unlike the PBC case, there is no reflection symmetry, due to the SPBC. In the steady state, all C's in each group must be equally probable, leaving us with only 4 P^*'s.

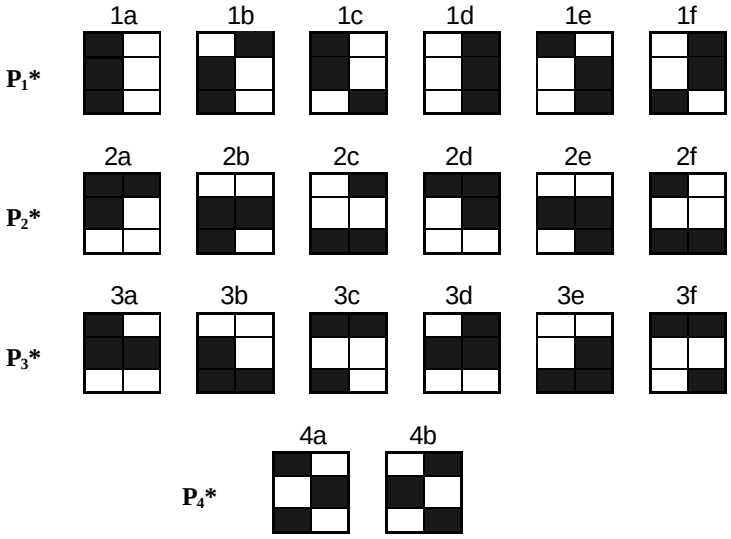

Figure 2.2 Probabilities for Groups of Configurations in a 2×3 Lattice with SPBC

Focusing on $E = \infty$ and finite T, the Master equation (2.2), with zero on the left, can be easily solved. Defining $x \equiv e^{-\beta J}$, the normalized distribution is

$$\begin{aligned} P_1^* &= 3/\left(44 + 16x^2\right) \\ P_2^* &= P_3^* = \left(2 + x^2\right)/\left(44 + 16x^2\right) \\ P_4^* &= \left(1 + 2x^2\right)/\left(44 + 16x^2\right) \end{aligned}$$

where the subscript refers to the groups in Figure 2.2. These assume the form

$$P_{eq1}^* = x/Z, \quad P_{eq2}^* = P_{eq3}^* = 1/Z; \quad P_{eq4}^* = x^3/Z; \quad Z = 12 + 6x + 2x^3$$

for the $E = 0$ equilibrium case.

Clearly, these two distributions are quite different functions of T. Let us highlight a few points. As expected, all configurations are equally probable (1/20) for both systems at infinite temperature ($x = 1$). On the other hand, at the opposite extreme ($T = x = 0$), the undriven system displays phase separation (transverse to the drive, in this case). In contrast to both equilibrium and driven PBC cases, *none* of the P^*'s vanish for $E = \infty$ and $T = 0$ with SPBC. One consequence is the lack of *complete* (or maximal) phase separation. These are the

first indications that the *bulk* properties of a driven system may be significantly affected by imposing SPBC. As a final example of what interesting phenomena can be extracted out of such a simple system, we have computed the average (internal) energy $U \equiv < \mathcal{H} >$, its fluctuations $\Delta U^2 \equiv < \mathcal{H}^2 - U^2 >$, and the "specific heat" $\partial U/\partial T$. Just as in the PBC cases [22], the drive leads to one manifestation of the violation of the fluctuation dissipation theorem (FDT), i.e.,

$$\Delta U^2 \neq k_B T^2 \left(\partial U/\partial T\right)$$

the equality of the two quanities is guaranteed for systems in equilibrium.

Finally we turn to simulation studies, which allow us to explore the co-operative behavior of many-body systems and form the main part of this thesis. In this approach, our 72×36 systems are evolved in time, starting in either a random or completely ordered initial configuration. Here, "completely ordered" refers to having a solidly filled single strip of the appropriate width ρL, tilted appropriately to satisfy SPBC. Thus, these are the $T = 0$, $E = 0$ configurations, with two identical, sharp interfaces that consist of a series of "ledges" of equal length. Time evolution is quoted in Monte Carlo steps. During such a step, the system is updated by randomly choosing a nearest-neighbor pair (a bond) and implementing (2.6) if it is a particle-hole pair. Specifically, they will be exchanged provided the resultant $(-\beta\Delta\mathcal{H} + E\Delta j)$ is positive; otherwise, with probability $\exp\left(-\beta\Delta\mathcal{H} + E\Delta j\right)$. In the next two Chapters, we present our analysis of the disordered phase of the driven system followed by our determination of the co-existence curve, using several different methods.

3. TWO-PARTICLE CORRELATIONS IN THE DISORDERED PHASE

Though the most interesting phenomena in these systems are phase transitions, they do display non-trivial behavior, unlike their equilibrium counterparts, even in the disordered state. In particular, the two-point correlation is long ranged [23], despite the short ranged nature of both the interparticle interactions and the hopping dynamics. This chapter is devoted to a study of such correlations.

3.1. Microscopics of the Simulations and Typical Configurations

To simulate a model governed by the Master equation (2.2) with rates (2.6), we chose a 72×36 lattice. In the computer codes, we used the spin language, so that

$$s(i,j) = \pm 1 \tag{3.1}$$

for each site (i,j). To re-emphasize, shifted periodic boundary condition (SPBC) implies that the following pairs

$$\begin{aligned} &(1,j) \quad \text{and} \quad (72,j) \\ &(i,1) \quad \text{and} \quad (i+H,36) \end{aligned} \tag{3.2}$$

are nearest neighbors. In general, we have

$$(i,j) = (i+72,j) = (i+H,j+36) \tag{3.3}$$

For convenience, we investigated only systems with shifts which are divisors of the vertical length, i.e.,

$$H = 0,3,4,6,9, \text{ and } 18\ . \tag{3.4}$$

For this part of our study, only half-filled systems are used, i.e.,

$$\sum_{i,j} s(i,j) = 0. \tag{3.5}$$

Finally, we selected three temperatures: from a "high" of 4.0 (in units of the Onsager temperature) to just above criticality, which are slightly different for the various shifts. In the driven cases, only infinite E was used. An $E = 0$ case was also included, for convenient comparisons with the equilibrium model. In the simulations, $E = \infty$ is actually $50J$.

Since we are focussing on disordered states, an initially random configuration is chosen. In a Monte Carlo step , one of the $72 \times 36 \times 2$ "bonds" (i.e., pairs of nearest neighboring spins) is randomly chosen for update. In this manner, on the average each bond has the same chance of being chosen in a step. Clearly, if the chosen pair are of equal signs, exchanges are unnecessary. If they are of opposite signs, we compute the change in both the internal energy and the "local potential" due to E:

$$\Delta \equiv -\beta \Delta \mathcal{H} + E \Delta j \tag{3.6}$$

and, according to (2.6), exchange the pair with "probability" $\min\{1, \exp(\Delta)\}$. The Monte Carlo "second" (MCS) is defined to be $72 \times 36 \times 2$ Monte Carlo steps. Typical runs are 100K MCS long. Given that the transients in the system will usually die down in 20K MCS, we take measurements on 400 configurations in the last 80K MCS. It is generally believed that configurations separated by 200 MCS are no longer correlated. Figures 3.1a-f show the typical configurations for systems driven into steady states (as exhibited by correlations studies), subjected to various shifts and temperatures.

(a) T=0.4 (b) T=2.0 (c) T=1.5

Figure 3.1(a) Typical configurations for $H = 0$

(a) T=4.0 (b) T=2.0 (c) T=1.4

Figure 3.1(b) Typical configurations for $H = 3$

(a) T=4.0 (b) T=2.0 (c) T=1.4

Figure 3.1(c) Typical configurations for $H = 4$

(a) T=4.0 (b) T=2.0 (c) T=1.3

Figure 3.1(d) Typical configurations for $H = 6$

(a) T=4.0 (b) T=2.0 (b) T=1.5

Figure 3.1(e) Typical configurations for $H = 9$

(a) T=4.0 (b) T=2.0 (c) T=1.5

Figure 3.1(f) Typical configurations for $H = 18$

3.2. Two-point Correlations in Systems with PBC and SPBC

Since there is no spontaneous symmetry breaking above criticality, the most prominent feature of our statistical system is the two-point correlation. Due to translational invariance, only the relative co-ordinate between the two spins are needed, so that we write

$$G(x, y) \equiv < s(0, 0)s(x, y) > \tag{3.7}$$

which carries information on the probability that the two spins are aligned. In a simulation study, $< \ldots >$ will be computed through averages both in space and

time. Explicitly, the former involves

$$\frac{1}{V}\sum_{i,j} s(i,j)s(i+x,j+y) \tag{3.8}$$

with $V = LM = 2592$ here. We should emphasize that SPBC (3.3) must be used if the arguments in $s(i+x, j+y)$ exceed (72,36). The time average is simple, using the 400 configurations in the last 80K MCS.

Before displaying the results, let us examine the symmetry properties of (3.7). We have, with PBC,

$$G(x,y) = G(-x,-y) \tag{3.9}$$

which may be called "inversion" symmetry. Note that this is an *exact* symmetry, obeyed configuration by configuration. Of course, in the special case of $y = 0$, this symmetry is same as reflection symmetry: $x \to -x$. For a system in equilibrium or a driven one, with $H = 0$, we could expect invariance under that symmetry also, i.e.,

$$G(x,y) = G(-x,y) \tag{3.10}$$

for arbitrary y. However, this symmetry holds only *on the average*. For the driven system with SPBC, there are no general arguments for (3.10) to be true.

Finally, we note that the case of $y = M/2$ is special, like the $y = 0$ PBC case. There is an exact reflection symmetry, around the shifted axis: $x = H/2$. To see this, we use (3.3) and obtain

$$G(x+\frac{H}{2},\frac{M}{2}) = G(x-\frac{H}{2},-\frac{M}{2})$$

so that, by (3.9),

$$G(x+\frac{H}{2},\frac{M}{2}) = G(-x+\frac{H}{2},\frac{M}{2}). \tag{3.11}$$

While it is the traditional quantity, this G may not be the most convenient for displaying order along the shifted axes. Since it must satisfy SPBC, a plot of its contours is expected to display a sheared character. Thus, we are led to define a *skewed* correlation function:

$$\tilde{G}(\tilde{x},\tilde{y}) \equiv G(x-\lambda y, y) \tag{3.12}$$

so that its contour plots satisfy PBC in the *sheared* co-ordinates

$$\tilde{x} \equiv x - \lambda y, \qquad \tilde{y} \equiv y \tag{3.13}$$

where

$$\lambda \equiv H/M$$

In particular, for a completely ordered state with a single tilted strip (e.g., in the $T = E = 0$ case with SPBC), it would be invariant under both parity and reflection:

$$\tilde{G}(\tilde{x}, \tilde{y}) = \tilde{G}(-\tilde{x}, -\tilde{y}) = \tilde{G}(-\tilde{x}, \tilde{y}) = \tilde{G}(\tilde{x}, -\tilde{y}).$$

Note that, since G is defined only for integer values of (x, y), $\tilde{G}$ will not "lie" on a square lattice. What these two correlation functions emphasize is the competition between the drive and the boundary condition. In particular, we will discuss the roles played by G and $\tilde{G}$ in displaying the significant differences between the $H = 4$ and 18 cases. In Figures 3.2a-f and 3.3b-f, we show contour plots of both G and $\tilde{G}$ for the states associated with configurations shown in Figs. 3.1a-f. For visibility in these plots, the normalization factor $1/V$ in (3.8) is suppressed.

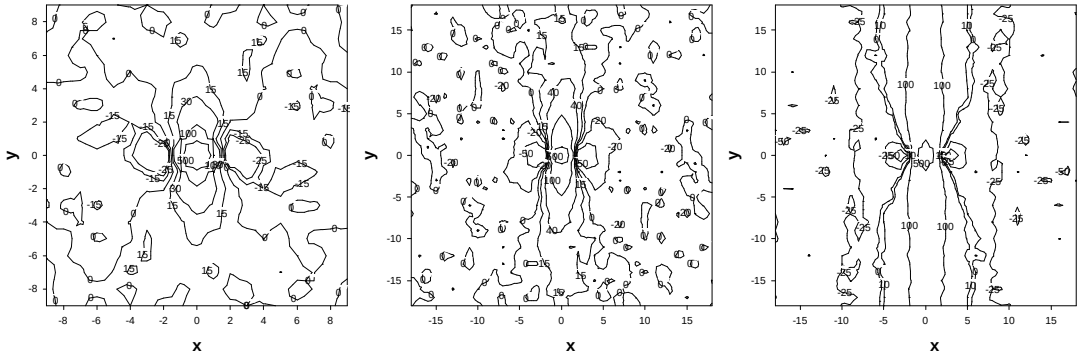

(i) T=4.0 (ii) T=2.0 (ii) T=1.5

Figure 3.2 (a) Contour Plot of G(x,y) for H=0

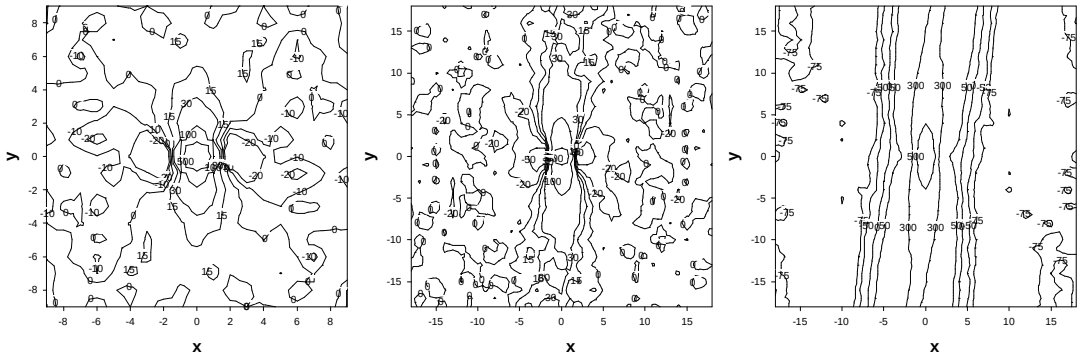

(i) T=4.0 (ii) T=2.0 (c) T=1.3

Figure 3.2 (b) Contour Plot of G(x,y) for H=3

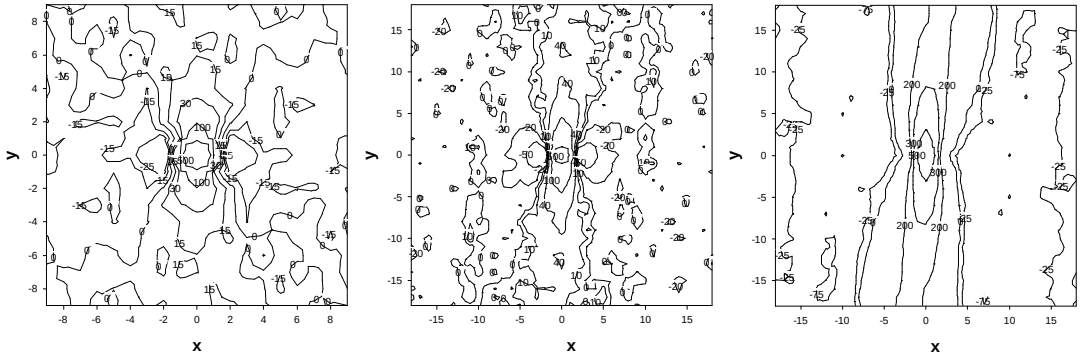

(i) T=4.0 (ii) T=2.0 (iii) T=1.3

Figure 3.2 (c) Contour Plot of G(x,y) for H=4

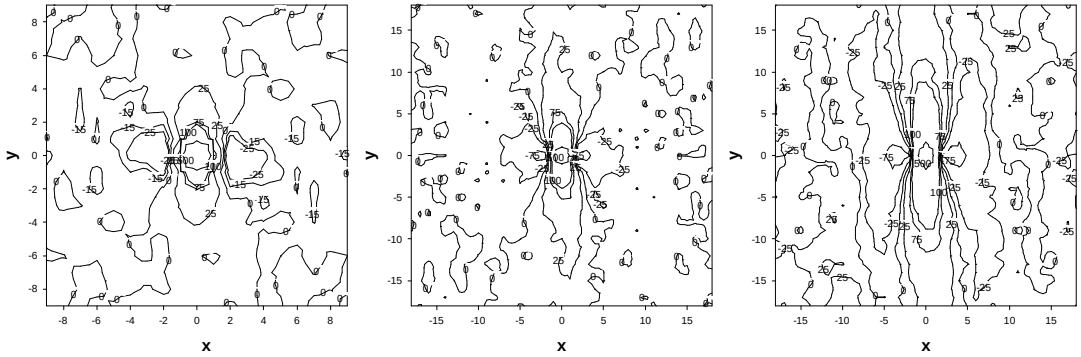

(i) T=4.0 (ii) T=2.0 (iii) T=1.3

Figure 3.2 (d) Contour Plot of G(x,y) for H=6

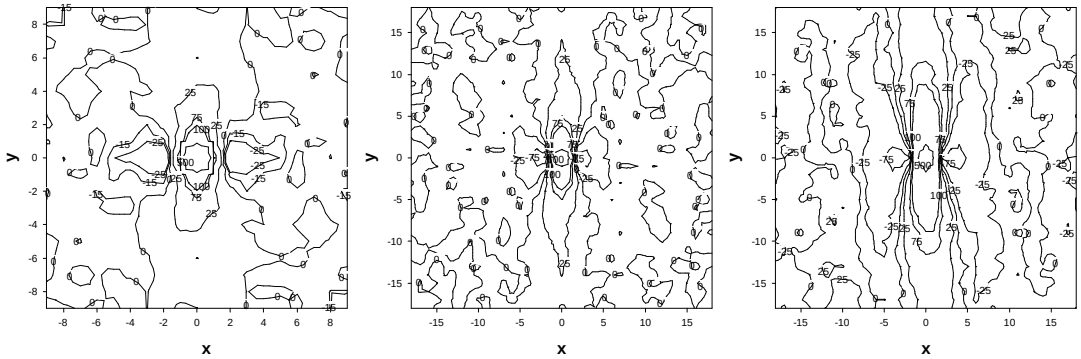

(i) T=4.0 (ii) T=2.0 (iii) T=1.5

Figure 3.2 (e) Contour Plot of G(x,y) for H=9

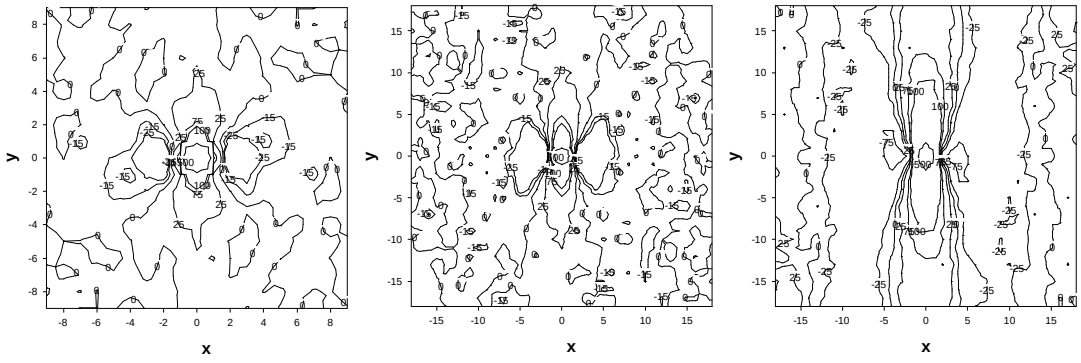

(i) T=4.0 (ii) T=2.0 (iii) T=1.5

Figure 3.2 (f) Contour Plot of G(x,y) for H=18

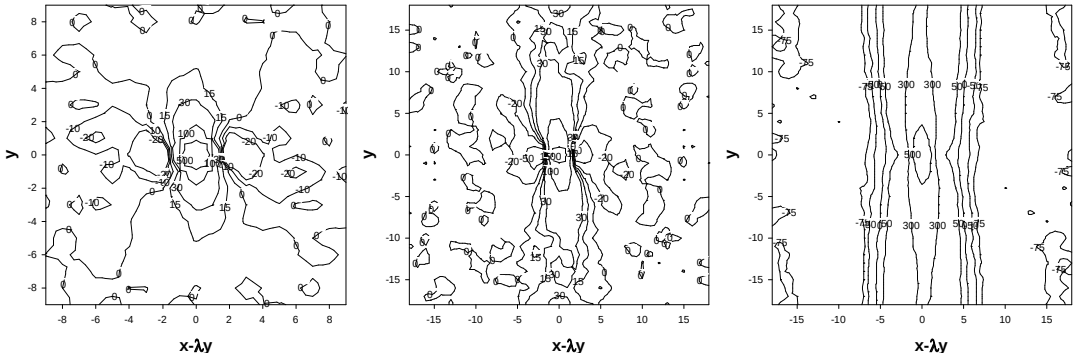

(i) T=4.0 (ii) T=2.0 (iii) T=1.3

Figure 3.3 (b) Contour Plot of $\widetilde{G}(x, y)$ for H=3

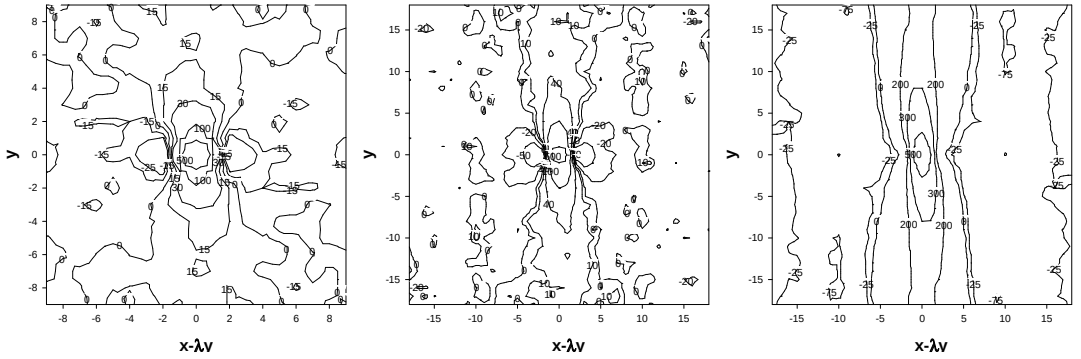

(i) T=4.0 (ii) T=2.0 (iii) T=1.3

Figure 3.3 (c) Contour Plot of $\widetilde{G}(x, y)$ for H=4

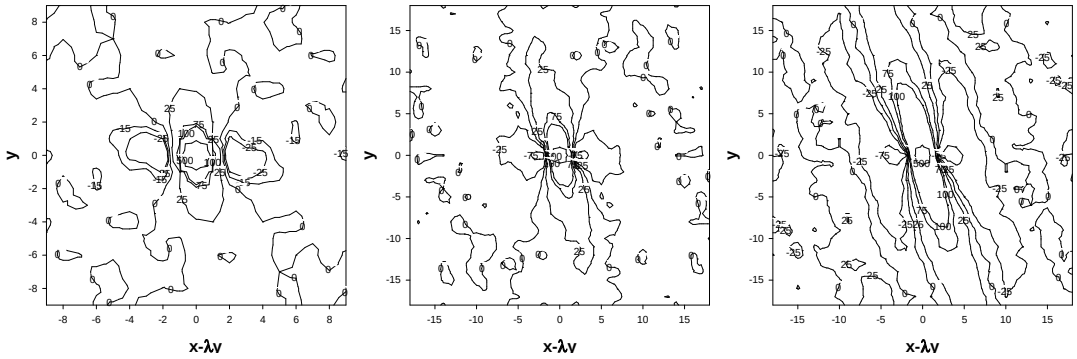

(i) T=4.0 (ii) T=2.0 (iii) T=1.3

Figure 3.3 (d) Contour Plot of $\widetilde{G}(x, y)$ for H=6

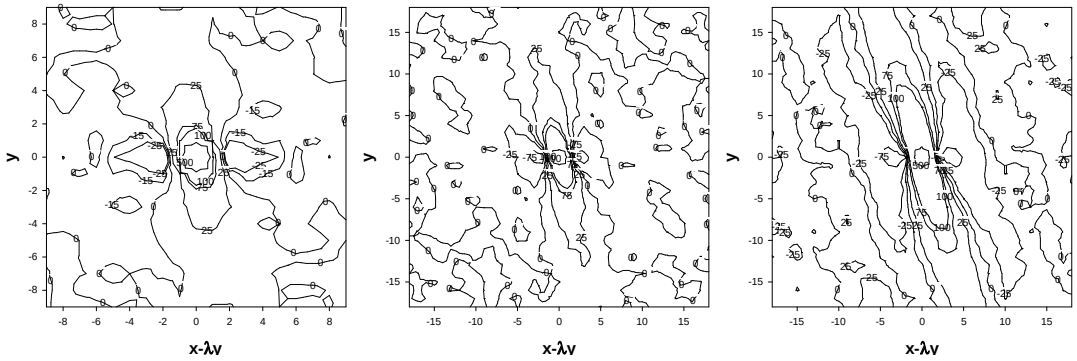

(i) T=4.0 (ii) T=2.0 (iii) T=1.5

Figure 3.3 (e) Contour Plot of $\widetilde{G}(x, y)$ for H=9

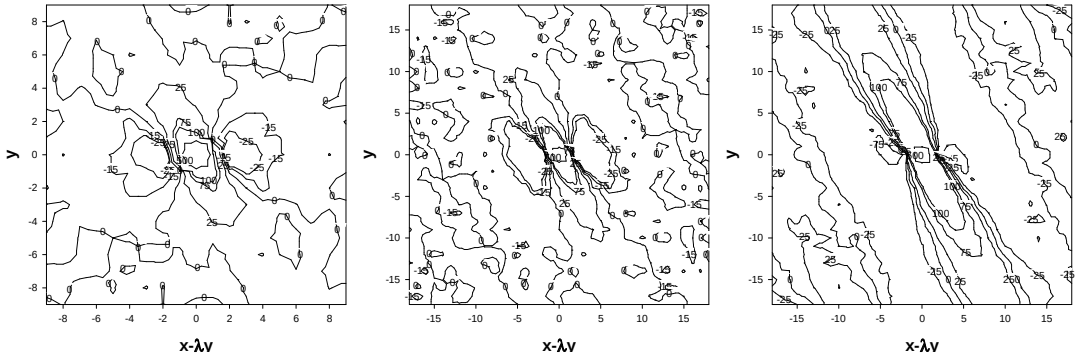

(i) T=4.0 (ii) T=2.0 (iii) T=1.5

Figure 3.3 (e) Contour Plot of $\widetilde{G}(x, y)$ for H=18

Note that, for the high temperature ($T = 4$) cases, the correlation is so short in range that we limit the plots to $[-9, 9]$. By contrast, for the other two temperatures, the full range of $y \in [-18, 18]$ is used. For simplicity, we choose the same range for x or $\tilde{x}$.

Finally, as a comparison, we also show plots for the equilibrium case (Figure 3.4).

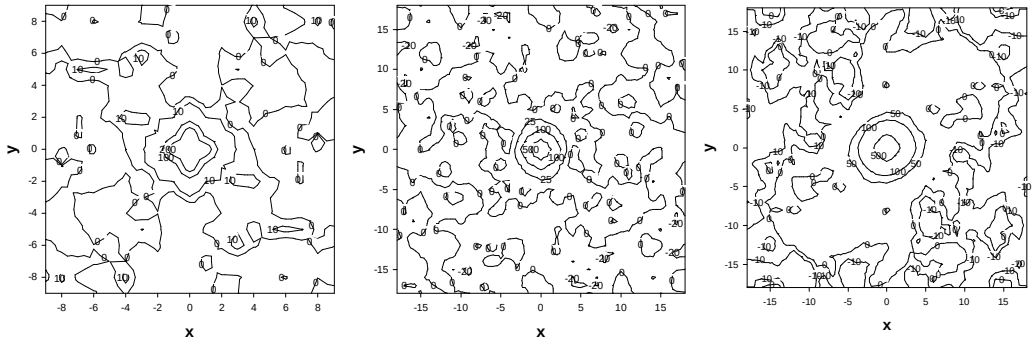

(a) T=4.0 (b) T=2.0 (c) T=1.5

Figure 3.4 Contour plot of $G(x, y)$ for an equilibrium system with PBC.

Not surprisingly, in the driven systems, correlations are highly anisotropic, being positive along the field and negative in the transverse direction. They are clearly stronger than in the $E = 0$ case, but correlations are not an efficient way to measure quantitatively the long ranged nature of the correlations. The large distance effects are more transparent through the structure factors, the topic of the next section. Here, let us point out some interesting features.

For a system in *equilibrium*, we should expect that, in the neighborhood of $(0, 0)$, correlations should not be much affected by the boundary conditions. In particular, the correlation length is small far above criticality, so that SPBC makes little impact on the correlation function. Thus, we expect that G would be quite adequate. On the other hand, as we approach T_c and the correlation length reaches the system size, SPBC will undoubtedly make its presences felt, so that using $\tilde{G}$ would be more convenient.

In contrast, the situation is more complex for a *driven system*.

For very high temperatures, there is little correlation in general and we may expect that G or $\tilde{G}$ will be significant only near the origin. Thus, the effects of SPBC are expected to be minimal. From the $T = 4$ plots in Figs. 3.2, which show the G's up to $|x|, |y| = 9$, the contours are essentially independent of the

shift. Of course, this also means that the corresponding plots for the $\tilde{G}$'s (Figs. 3.3) become increasingly slanted for large H.

For intermediate T's, the effects of $H \neq 0$ are already discernible, since the correlations are longer-ranged. As T is lowered towards criticality, these effects are not only quite pronounced, they lead us to the distinction between low and high shift states. The reason lies in the dipolar form of the long-range correlations, i.e., power law decays with a positive/negative amplitude along/transverse to the drive [23, 24]. Although all previous studies of correlations are based on systems with PBC, we may assume that this alignment with E continues to hold even with SPBC. The result is a competition between E, which favors the lattice orientation spiralling down the torus, and the *interparticle interactions,* which favors the orientation imposed by the SPBC (See Fig. 2.1). Certainly, this competition is responsible for the phenomena of ordered states with multistrips below criticality [15]. In that case, there are significant differences between "low shifts" ($H/M \lesssim 10/100$) and "high" ones ($H/M \gtrsim 15/100$). Here, with $M = 36$, similar important differences between "low shifts" ($H = 3, 4$) and "high" ones ($H = 9, 18$) are clearly seen within the *disordered* states. Especially for the systems at the lower T, we see that, for low shifts, the contours near the origin are aligned more vertically in G, but the contours farther from the origin are aligned more vertically in $\tilde{G}$. However, for high shifts, essentially all parts of the contours are slanted in $\tilde{G}$, even though they are constructed to satisfy PBC in these plots! By contrast, they are basically vertical in G. This difference between the $H = 3, 4$ and $9, 18$ plots demonstrates that, for large H/M, the drive exerts a more profound influence and the particles simply cluster into strips aligned with E but multiply wound around the torus to accommodate the SPBC. These results are clearly consistent with multistrip states in systems subjected to large shifts and low temperatures.

This competition between E and J is obviously less dramatic at high temperatures. In fact, the power law gives way to a constant *negative* correlation, due to the conservation law in a finite system [3]. As a result, the dominant features in the $T = 4$ cases are just the anisotropic correlations near the origin. Clearly, there is a rich crossover phenomenon, from the high T regime to near criticality, since there are drastic differences between high and low shifts at low temperatures. A much more extensive study will be necessary to explore these complexities.

3.3. Ordinary and Skewed Structure Factors

In this section, we study the large distance behavior of correlation functions, which are expected to display power law decays. Instead of finding (3.7) for large values of (x, y) and fitting the curves, a better method relies on measuring the Fourier transforms, namely, the structure factors. With PBC ($H = 0$), the definition is standard:

$$S(\mathbf{k}) = \sum_{\mathbf{x}} < s(\mathbf{0})s(\mathbf{x}) > e^{i\mathbf{k}\cdot\mathbf{x}} \tag{3.14}$$

where $\mathbf{x} = (x, y)$ and

$$\mathbf{k} = (k_x, k_y) = 2\pi \left(\frac{n_x}{L}, \frac{n_y}{M}\right) \tag{3.15}$$

with

$$\begin{aligned} n_x &= 0, 1, \ldots, L-1 \\ n_y &= 0, 1, \ldots, M-1. \end{aligned} \tag{3.16}$$

In fact, this is also a more *efficient* method, since (3.14) can be obtained from measuring

$$f(\mathbf{k}) = \frac{1}{\sqrt{V}} \sum_{\mathbf{x}} s(\mathbf{x}) e^{i\mathbf{k}\cdot\mathbf{x}} \tag{3.17}$$

first and then performing only the "time" average over $|f(\mathbf{k})|^2$, i.e.,

$$S(\mathbf{k}) \equiv \left\langle |f(\mathbf{k})|^2 \right\rangle_t . \tag{3.18}$$

This is the "ordinary" structure factor. Of course, our interest will be in the behavior of S's at low $\mathbf{k}$, since they dominate the large $\mathbf{x}$ properties of $G(\mathbf{x})$.

For systems with SPBC, however, it is not immediately obvious that eqns. (3.14)-(3.18) remain meaningful. There is no question that, if we were to cut our toroidal sample and lay it flat, as we will do in presenting configurations here, then these are the formulae for predicting the result of, say, light scattering therefrom. However, it is also clear that such a procedure introduces an "artificial" discontinuity in the configuration, i.e., the cut. Another perspective is to recall that eqns. (3.14)-(3.18) are valid for an infinite system formed by tiling, *periodically*, with the "cut-lattice". In such an infinite system, nearest neighbors across the (horizontal) cuts are not nearest neighbors in the original lattice: (3.2).

From a third perspective, the difficulty with (3.17) is that the basis set, $e^{i\mathbf{k}\cdot\mathbf{x}}$ with (3.15,3.16), does not satisfy the correct boundary conditions. Instead, we should construct a set which does satisfy (3.3). The result is $e^{i\bar{\mathbf{k}}\cdot\mathbf{x}}$ where

$$\bar{\mathbf{k}} = (\tilde{k}_x, \tilde{k}_y) = 2\pi \left(\frac{n_x}{L}, \frac{n_y}{M} - \frac{n_x H}{LM} \right) \tag{3.19}$$

with integer n's (3.16). Since $s(\mathbf{x})$ satisfies SPBC by construction, it can be expanded in this complete set of functions which also satisfy SPBC:

$$s(\mathbf{x}) = \sum_{\mathbf{k}} f(\bar{\mathbf{k}}) \frac{e^{-i\bar{\mathbf{k}}\cdot\mathbf{x}}}{\sqrt{V}} \quad . \tag{3.20}$$

Noting that, due to

$$\sum_{\mathbf{x}} e^{-i\bar{\mathbf{k}}'\cdot\mathbf{x}} e^{i\bar{\mathbf{k}}\cdot\mathbf{x}} = V \delta_{\bar{\mathbf{k}}',\bar{\mathbf{k}}} \quad ,$$

$e^{i\bar{\mathbf{k}}\cdot\mathbf{x}}/\sqrt{V}$ is still an orthonormal set, we have

$$f(\bar{\mathbf{k}}) = \frac{1}{\sqrt{V}} \sum_{\mathbf{x}} s(\mathbf{x}) e^{i\bar{\mathbf{k}}\cdot\mathbf{x}} \quad . \tag{3.21}$$

To emphasize, although this expression appears to be the same as (3.17), they are actually different, since the allowed $\bar{\mathbf{k}}$'s are given by (3.19) here, rather than the $\mathbf{k}$'s of (3.15) above.

Given a sensible Fourier representation for the configuration, (3.20, 3.21), we can study the amplitudes (and phases) of f. In particular, following the steps for PBC, we can just define *skewed structure factors* by

$$\tilde{S}_H(n_x, n_y) \equiv \left\langle |f(\bar{\mathbf{k}})|^2 \right\rangle_t \quad . \tag{3.22}$$

Note that we have included a subscript, to indicate the specific shift associated. The information contained in (3.22) is, of course, the same as that in (3.18) for an *infinite* system with continuous $\mathbf{x}$. For finite discrete systems, however, the difference is probably best seen through a comparison diagram (Fig. 3.5) in which we have identified the allowed wave-vectors for the two cases.

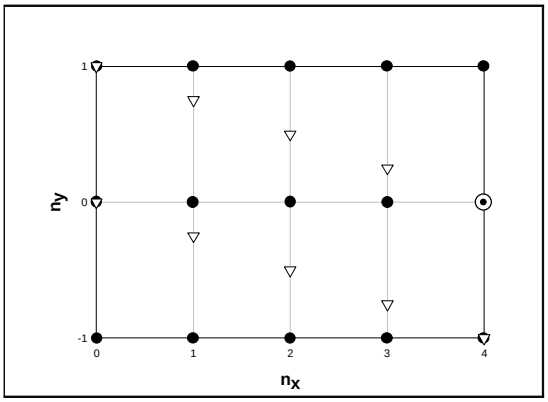

Figure 3.5 Allowed values in the space of wave-vectors for $H = 18$. Dots(triangles) are associated with ordinary(skewed) structure factors.

To appreciate this comparison, we have circled a single component which is represented differently, namely, $S(4,0) = \tilde{S}_{18}(4,1)$. In Table 3.5, we see that these two entries contain identical values. Further symmetry properties and an example of S and $\tilde{S}_4$ for the completely ordered state at half filling may be found in Appendices B and C.

With these remarks in mind, we turn to the data. In this chapter, only half-filled systems have been used, so that $S(0,0) = \tilde{S}_H(0,0) \equiv 0$ in all cases. As a test of our simulations, we first represent, in Tables 3.1a and b, the data for systems with PBC ($H = 0$) at $T = 1.5$, both in equilibrium and under the drive ($E = \infty$). Of course, there is no need to study $\tilde{S}$ here.

Table 3.1 (a) $S(\mathbf{k})$ for E=0, T=1.5, H=0

$n_y \backslash\ n_x$	0	1	2	3	4	5	6	7	8	9
0	0.0	6.6	6.8	5.9	5.1	5.1	4.2	3.8	3.6	3.1
1	5.7	6.7	6.6	6.0	5.4	4.5	4.4	3.5	3.2	2.9
2	5.2	5.5	5.0	5.0	4.5	4.1	3.6	3.2	2.8	2.6
3	4.1	4.0	4.3	4.0	3.6	3.5	3.0	2.7	2.5	2.4
4	3.2	3.2	3.2	3.2	3.0	2.7	2.6	2.3	2.3	2.1
5	2.6	2.7	2.8	2.5	2.2	2.2	2.2	2.0	1.9	1.7
6	2.3	2.0	2.0	2.0	2.0	1.8	1.9	1.8	1.7	1.4
7	1.7	1,7	1.7	1.6	1.6	1.6	1.5	1.4	1.3	1.4
8	1.5	1.4	1.4	1.4	1.4	1.4	1.3	1.3	1.2	1.2
9	1.2	1.3	1.2	1.3	1.2	1.1	1.2	1.2	0.9	1.0

Table 3.1 (b) $S(\mathbf{k})$ for E=∞, T=1.5, H=0

$n_y \backslash\ n_x$	0	1	2	3	4	5	6	7	8	9
0	0.0	17.9	22.7	16.0	14.2	11.2	8.8	7.7	6.3	5.4
1	1.3	1.5	1.6	2.1	2.6	3.2	3.6	3.4	3.8	3.6
2	0.9	1.0	1.1	1.2	1.5	1.9	2.0	2.1	2.3	2.4
3	0.8	0.9	1.0	1.0	1.1	1.3	1.3	1.3	1.6	1.7
4	0.8	0.9	0.9	0.8	1.0	0.9	1.2	1.2	1.2	1.3
5	0.7	0.7	0.8	1.0	0.9	0.9	1.0	1.0	1.1	1.1
6	0.8	0.7	0.8	0.8	0.7	0.9	1.0	0.9	0.9	1.1
7	0.8	0.8	0.8	0.8	0.8	0.8	0.8	0.9	0.9	0.8
8	0.7	0.8	0.8	0.9	0.8	0.8	0.8	0.9	0.9	0.9
9	0.8	0.7	0.8	0.8	0.8	0.8	0.8	0.8	0.8	0.8

For the equilibrium case, S is more or less isotropic, peaking near the origin. To discern this property, we emphasize that these entries must be examined with Fig. 3.5 in mind, so that, e.g., $S(2,0)$ should be compared to $S(0,1)$. Anticipating a Ornstein-Zernike form for $S(\mathbf{k})$, we see that $S(1,0)$ will be the largest component, just because it is closer to the origin. Unlike the driven case, any systematic deviation of the ratio $S(1,0)/S(0,1)$ from unity is *not* a signal of the violation of the fluctuation dissipation theorem! Since no discontinuity is expected at $\mathbf{k} = \mathbf{0}$, this ratio will approach unity in the thermodynamic limit. However, as T is lowered to 1, we can expect $S(1,0)$ to "diverge" first, signaling order in a state with a single strip aligned vertically. This behavior is entirely consistent with the system assuming a state with minimal surface energy.

In sharp contrast, S is strongly anisotropic for the driven system, as expected. Dominated by the purely transverse components ($n_y = 0$), it displays the finite *discontinuity singularity* at the origin [24], whether we compare $S(1,0)$ or $S(2,0)$ to $S(0,1)$. To be consistent with equilibrium cases, we will focus on the ratio

$$R \equiv \frac{S(2,0)}{S(0,1)}. \tag{3.23}$$

In Table 3.2, we present R for these systems for $T = 1.5, 2.0$, and 4.0. In these runs, with an initially random state, the system is first set at $T = 4.0$ and evolved for 100K MCS. For each of the subsequent temperatures, the system is evolved for a further 100K MCS *without resetting* the configuration to random. As usual, for each segment, only the final 80K MCS are used for computing averages. By this method, it is hoped that the lowest temperature studied will be more likely to be in a steady state after (the discarded) 20K MCS. The reason for choosing $T = 1.5$ is that, for the driven case, long range order is known to set in at $T \simeq 1.41$[26].

In all cases, there is no question that, within the errors, R is equal to and distinct from unity for, respectively, the $E = 0$ and $E = \infty$ cases.

Table 3.2 R for equilibrium and driven systems with PBC

$E\backslash T$	4.0	2.0	1.5
0	1.01	0.94	1.20
∞	1.75	4.31	18.16

The significance of $R \neq 1$ and its relevance to power law decay of correlations is understood [24], so that the connection will not be re-iterated here. What we have found is simply a confirmation of this well known property in driven systems with PBC. As a further test of our simulations, we have compiled histograms from the 400 samples of $|f(\mathbf{k})|^2$ in each run. We verified that these are well approximated by an exponential distribution, which is the expected behavior in a disordered state far from criticality [31]. The values shown in all the Tables are averages over these distributions.

Finally, we turn to driven systems with non-trivial shifts. For each H, the methods used are the same as above: starting with a random configuration, the system is quenched to $T = 4.0$ for 100K MCS and subsequently, without resetting the configurations, cooled to 2.0 and then a temperature believed to be slightly above criticality. As we will see in the next chapter, ordering does not set in at the same T for systems with different H. In all runs and for each T, we evolved the systems for 100K MCS and used the last 80K MCS for measurements (so that the sample size is always 400).

As in the PBC cases, to get a more detailed picture of these structure factors, we compiled histograms of their $|f(\mathbf{k})|^2$ distributions. All are consistent with being exponentially distributed. Figures 3.6 and 3.7 show the histograms for selected structure factors for the $H = 4$ and 18 cases. The H=4 case shows the skewed structure factors at three different temperatures. Figure 3.7 compares ordinary structure factors to the skewed ones at T=1.5.

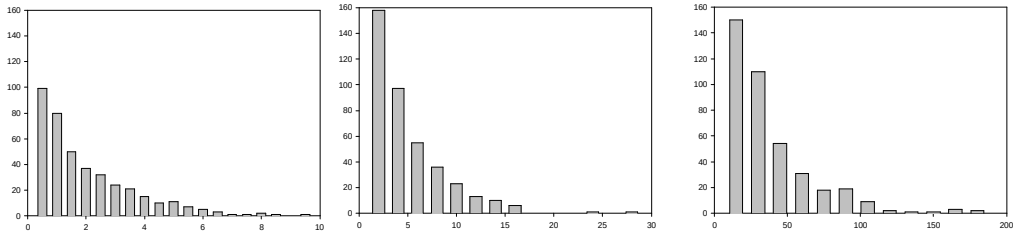

(a) $\tilde{S}(1,0)$ T=4.0 (b) $\tilde{S}(1,0)$ T=2.0 (c) $\tilde{S}(1,0)$ T=1.3

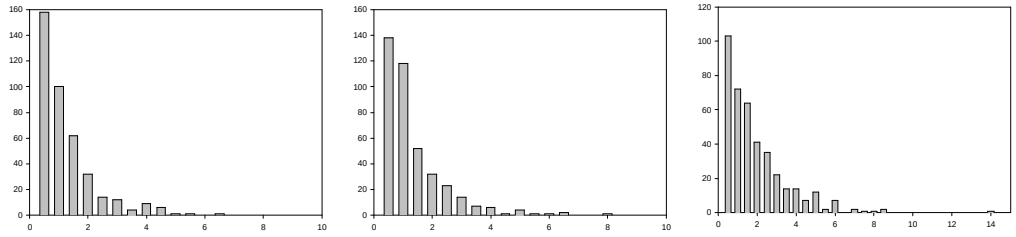

(d) S(0,1) T=4.0 (e) S(0,1) T=2.0 (f) $\tilde{\mathrm{S}}$(0,1) T=1.3

Figure 3.6 Histograms for S(1,0) and S(0,1) for H=4, $T > T_c$

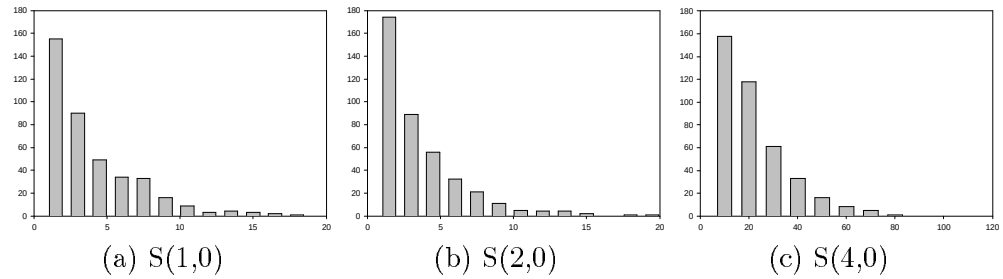

(a) S(1,0) (b) S(2,0) (c) S(4,0)

(d) $\widetilde{S}_{18}$(1,0) (e) $\widetilde{S}_{18}$(2,0) (f) $\widetilde{S}_{18}$(4,0)

Figure 3.7 Histograms for Some Structure Factors for $H = 18$, T=1.5

As we see, imposing SPBC has no drastic effect on the *shape* of these distributions. Instead of fitting these to exponentials, which requires better statistics and longer runs, we compute only the averages and standard deviations. The latter, denoted by ΔS or $\Delta \tilde{S}_H$, would be identical to the averages (S or $\tilde{S}_H$) for an exponential distribution. Thus, comparing these quantities would provide a good indication of the expected distribution. As an example, we show in Tables 3.3 these quantities, only for the two lowest skewed structure factors, for all shifts. In all cases, these quantities are equal within statistical errors

Table 3.3 (a) Statistics for $\tilde{S}_H$ in systems with low shifts

	$H=0$			$H=3$			$H=4$		
statistic	$T=4.0$	2.0	1.5	4.0	2.0	1.3	4.0	2.0	1.3
$\tilde{S}_H(1,0)$	1.81	5.05	21.44	1.81	4.78	28.61	1.75	3.91	30.90
$\Delta\tilde{S}_H(1,0)$	1.77	5.13	21.46	1.76	4.93	32.35	1.64	3.77	29.87
$\tilde{S}_H(0,1)$	0.96	1.08	1.25	0.93	1.17	1.61	0.99	1.07	1.66
$\Delta\tilde{S}_H(0,1)$	0.91	1.11	1.67	0.85	1.14	1.51	1.01	1.09	1.64

Table 3.3 (b) Statistics for $\tilde{S}_H$ in systems with high shifts

	$H=6$			$H=9$			$H=18$		
statistic	$T=4.0$	2.0	1.3	4.0	2.0	1.5	4.0	2.0	1.5
$\tilde{S}_H\ (1,0)$	1.87	4.33	13.80	1.55	3.83	7.55	1.45	2.17	3.70
$\Delta\ \tilde{S}_H\ (1,0)$	1.68	4.28	13.87	1.49	3.56	7.09	1.45	1.96	3.46
$\tilde{S}_H\ (0,1)$	0.98	1.08	1.69	0.97	1.05	1.68	1.03	1.13	1.40
$\Delta\tilde{S}_H\ (0,1)$	0.97	1.17	1.62	1.02	1.14	1.70	0.95	1.10	1.34

With some confidence in the measurements of the structure factors, we first consider those with wave vectors near zero, since these are the ones which dominate the correlations at large distances. In particular, we quote in Table 3.4 the values for the ratios R (3.23) and

$$\tilde{R} \equiv \frac{\tilde{S}_H(2,0)}{\tilde{S}_H(0,1)}. \tag{3.24}$$

Table 3.4 The ratios (3.23) and (3.24) for all systems.*$T=1.3$ for $H=3,4,6$

$T \setminus H$	0	3		4	
	R	R	$\tilde{R}$	R	$\tilde{R}$
4.0	1.75	2.03	2.08	1.75	1.77
2.0	4.31	3.76	3.84	4.31	4.50
1.5/1.3*	18.16	27.49	28.13	17.96	18.62

$T \setminus H$	6		9		18	
	R	$\tilde{R}$	R	$\tilde{R}$	R	$\tilde{R}$
4.0	1.78	1.87	1.91	2.01	1.50	1.51
2.0	3.56	3.76	2.90	3.26	1.68	2.09
1.5/1.3*	8.04	8.68	4.13	4.78	1.99	2.34

As expected, these ratios are all greater than unity by sufficiently significant amounts. Though there are minor differences between R and $\tilde{R}$, we may declare that the violation of the fluctuation dissipation theorem continues to hold in all systems with SPBC and that long range correlations are present. Given $\tilde{S}_H(0,1) \equiv S(0,1)$, the fact that $\tilde{R} > R$ in all cases may be an indication of the higher sensitivity of $\tilde{S}_H(2,0)$ to particle correlations along the skewed direction.

Next, we turn to structure factors at higher wave numbers. These will turn out to carry significant amounts of the total "intensity" ($\sum_{\mathbf{k}} S(\mathbf{k}) = VG(\mathbf{0}) \equiv V$). One of the effects of the SPBC is that some ordered states consist of multistrips, especially for high H. In the disordered state, the precursors of this type of ordering are increased intensities in structure factors with higher $\mathbf{k}$. Table 3.5 shows both S and $\tilde{S}_4$ for $n_x \in [0,9]$ and $n_y = 0, 1$, in a low shift system for various temperatures.

Table 3.5 Ordinary and skewed structure factors for $H = 4$

$n_y \backslash\ n_x$	0	1	2	3	4	5	6	7	8	9
	$S(n_x, n_y)$ at $T = 4.0$									
0	0.0	1.75	1.73	1.67	1.76	1.79	1.71	1.63	1.68	1.67
1	.99	1.03	1.31	1.60	1.64	1.62	1.70	1.74	1.52	1.53
	$\tilde{S}_4(n_x, n_y)$ at $T = 4.0$									
0	0.0	1.75	1.75	1.67	1.76	1.84	1.80	1.87	1.76	1.66
1	.99	1.03	1.32	1.66	1.72	1.64	1.86	1.64	1.69	1.68
	$S(n_x, n_y)$ at $T = 2.0$									
0	0.0	3.90	4.61	4.12	3.77	3.72	3.47	3.29	2.91	3.19
1	1.07	1.32	1.79	2.43	2.69	2.83	2.95	2.70	2.56	2.63
	$\tilde{S}_4(n_x, n_y)$ at $T = 2.0$									
0	0.0	3.91	4.81	4.34	4.10	4.15	3.87	3.60	3.29	3.11
1	1.07	1.32	1.79	2.48	2.73	3.11	3.33	3.36	3.29	3.19
	$S(n_x, n_y)$ at $T = 1.3$									
0	0.0	30.57	29.81	27.74	20.92	15.05	11.10	7.89	6.10	5.28
1	1.66	1.80	2.23	3.02	3.86	4.16	4.65	4.93	4.55	3.67
	$\tilde{S}_4(n_x, n_y)$ at $T = 1.3$									
0	0.0	30.90	30.91	30.31	24.15	17.90	14.44	10.09	7.64	6.09
1	1.66	1.72	2.10	2.70	3.46	4.56	5.25	6.58	6.33	5.68

Note that $\tilde{S}_4 > S$ in essentially all cases, suggesting that there is considerable

clustering along the skewed co-ordinate. However, for large shifts, the picture is more complicated. The example of $H = 18$ is shown in Table 3.6.

Table 3.6 Ordinary and skewed structure factors for $H = 18$

$n_y \backslash n_x$	0	1	2	3	4	5	6	7	8	9
	$S(n_x, n_y)$ at $T = 4.0$									
0	0.0	1.47	1.55	1.77	1.78	1.67	1.67	1.71	1.67	1.76
1	1.03	1.08	1.28	1.38	1.51	1.66	1.61	1.56	1.73	1.59
	$\tilde{S}_{18}(n_x, n_y)$ at $T = 4.0$									
0	0.0	1.45	1.56	1.50	1.64	1.62	1.60	1.34	1.25	1.59
1	1.03	1.14	1.62	1.83	1.78	1.75	1.78	1.68	1.68	1.54
	$S(n_x, n_y)$ at $T = 2.0$									
0	0.0	1.98	1.90	3.49	4.47	3.99	3.44	3.21	3.71	3.92
1	1.13	1.36	1.72	1.84	2.19	2.85	2.54	2.59	2.85	2.90
	$\tilde{S}_{18}(n_x, n_y)$ at $T = 2.0$									
0	0.0	2.17	2.36	2.51	2.30	2.39	2.21	2.15	2.14	2.01
1	1.13	1.40	2.22	3.81	4.47	4.29	3.71	3.08	3.02	2.65
	$S(n_x, n_y)$ at $T = 1.5$									
0	0.0	3.23	2.79	8.22	16.45	9.05	5.53	6.25	7.33	5.02
1	1.40	1.67	1.97	2.53	2.60	4.25	4.31	3.70	4.42	4.17
	$\tilde{S}_{18}(n_x, n_y)$ at $T = 1.5$									
0	0.0	3.70	3.28	3.05	2.82	2.40	2.47	2.58	2.29	2.31
1	1.40	1.81	3.08	9.74	16.45	10.45	6.88	5.41	4.27	3.56

Several features are noteworthy here. Even at the highest T, $\tilde{S}_{18}(n_x, 0)$ is *rarely* greater than $S(n_x, 0)$. In fact, at $T = 1.5$, the dominant structure factor, $S(4, 0)$, is considerably greater than its counterpart: $\tilde{S}_{18}(4, 0)$. On the other hand, we see that it is identical to $\tilde{S}_{18}(4, 1)$! Recalling our discussion above concerning the relationship between S and $\tilde{S}$, this is not surprising. The large $S(4, 0)$ simply indicates that there is significant amount of clustering in the *vertical* direction, despite the system being subjected to SPBC. The constraints of the boundary conditions are eventually satisfied by multiple winding, which is reflected in the wave number $n_x = 4$. In the skewed representation, the multiple winding in one direction is necessarily accompanied by one in the other direction, leading to $n_y = 1$. The conclusion is obvious: even at a temperature far above T_c, the clusters are more affected by the drive than the SPBC and tend *not* to point in the

skewed direction. Certainly, at $T = 1.5$, the precursor to ordering into a multistrip state, aligned with E, is quite visible. On the other hand, it is remarkable that R_{18} is nevertheless greater than R, suggesting that the long range parts of the correlations continue to be affected more by the SPBC.

As a final measure of correlations along the skewed axes, we compare two other quantities. Let us define two averaged intensities:

$$< P_0 > \equiv \frac{1}{9} \left[\sum_{n_x=1}^{9} S(n_x, 0) \right] \tag{3.25}$$

and

$$< P > \equiv \frac{1}{99} \left[\sum_{n_x, n_y=0}^{9} S(n_x, n_y) \right] \quad . \tag{3.26}$$

Note that $S(0,0) = 0$ in the spin language, so that there are only 99 components in the latter sum. Similarly, we define averages for the shifted structure factors and denote them by $< \tilde{P}_0 >$ and $< \tilde{P} >$. The rationale behind these procedures is to have a measure that is relatively insensitive to clustering into multistrips. Of course, the former is more sensitive to the alignment of the vertical structures. If we expect strip-like clustering along the skewed axes, then $< P_0 >$ should be less than $< \tilde{P}_0 >$. On the other hand, if it is greater, then we may infer that there is significant amount of multiple winding, in order to satisfy SPBC and homogeneity in the original y co-ordinate. Table 3.7 displays the comparison between $< P_0 >$ and $< \tilde{P}_0 >$.

Table 3.7 (a) Power Comparison of $< P_0 >$ and $<\tilde{P}_0>$.*$T = 1.3$ for $H = 3, 4, 6$

$T \setminus H$	0	3		4	
	$< P_0 >$	$< P_0 >$	$< \tilde{P}_0 >$	$< P_0 >$	$<\tilde{P}_0>$
4.0	1.73	1.70	1.72	1.71	1.76
2.0	4.17	3.93	4.12	3.66	3.91
1.5/1.3*	12.93	21.71	23.40	17.16	19.16

$T \setminus H$	6		9		18	
	$< P_0 >$	$< \tilde{P}_0 >$	$< P_0 >$	$< \tilde{P}_0 >$	$< P_0 >$	$<\tilde{P}_0>$
4.0	1.67	1.87	1.70	1.71	1.67	1.50
2.0	3.47	3.76	3.41	3.26	3.24	2.25
1.5/1.3*	10.40	11.64	10.77	6.35	23.39	3.02

As we learn to expect, for low shifts, $< \tilde{P}_{\mathbf{0}} >$ is greater, implying that large scale correlations are more aligned with the skewed axes. On the other hand, for high shifts, the situation is completely reversed, showing better alignment with the unshifted axes.

As for $< P >$ vs. $< \tilde{P} >$, they obviously represent an even coarser gauge for the different types of alignment. In this sense, we may think of them as measures of the *general tendencies* of the large scale properties of particle correlations. Since the sum rule implies that the overall average intensity is unity, the difference between $< P >$ and $< \tilde{P} >$ translates into complementary differences at large $\mathbf{k}$ and therefore, at short distances. Table 3.7 displays the comparison between $< P >$ and$< \tilde{P} >$.

Table 3.3 (b) Power Comparison of $< P >$ and $< \tilde{P} >$.*$T = 1.3$ for $H = 3, 4, 6$

$T \setminus H$	0	3		4	
	$< P >$	$< P >$	$< \tilde{P} >$	$< P >$	$<\tilde{P}>$
4.0	1.16	1.15	1.16	1.16	1.18
2.0	1.45	1.48	1.51	1.45	1.51
1.5/1.3*	2.19	3.09	3.22	2.72	2.94

$T \setminus H$	6		9		18	
	$< P >$	$< \tilde{P} >$	$< P >$	$< \tilde{P} >$	$< P >$	$< \tilde{P} >$
4.0	1.15	1.18	1.16	1.21	1.15	1.22
2.0	1.42	1.52	1.42	1.55	1.39	1.58
1.5/1.3*	2.19	2.53	2.21	2.53	3.18	3.48

With this coarse measure, we see that $< \tilde{P} >$ is always the greater, regardless of shift. From these data, we infer that, at larger wave numbers, $S > \tilde{S}$ on the average. We interpret this behavior as correlations at short distances being controlled more by the field than the SPBC. These conclusions are entirely consistent with our picture of the competition between E and J, the former being dominant at short distances and the latter, at large distances, provided the shifts are low enough.

4. Densities of co-existing phases in half-filled systems

Since the microscopic dynamics of our system conserves particle number, the overall density of the system, $\overline{\rho}$, remains constant regardless of T. At critical density $\overline{\rho}_c$, a system is in a homogeneous phase as long as $T > T_c$. Below T_c, phase separation occurs, with co-existence of particle-rich and particle-poor regions. In the bulk of these regions, the densities will be ρ_+ and ρ_-, respectively. One definition of the co-existence curve is $\rho_\pm(T)$. For systems with densities $\bar{\rho} < \bar{\rho}_c$, the inhomogeneous, phase separated state does not appear until some temperature below T_c. The coexistence curve can also be defined as the line in the T-$\overline{\rho}$ plane which divides the disordered, homogeneous phase from the ordered, inhomogeneous one. In the thermodynamic limit, these two definitions are identical for systems in equilibrium. We expected them to be the same for driven systems also, despite both earlier claims and our own findings that there are differences. We believe that the differences are due to finite size effects, which are present even for systems in equilibrium. A systematic study of these effects, though crucial to finding a definitive answer to the co-existence curve, is beyond the scope of this thesis. Our goal is an estimate, to the accuracy of about 10%, of the co-existence curve.

Following the lead of [16] and [17], we investigate the phenomenon of co-existence, using their two methods. In this chapter, we focus on the first method, in which only the half-filled system (i.e., $\bar{\rho} = \bar{\rho}_c$) is studied. At various temperatures $T < T_c$, the densities of the particle-rich and particle-poor bulk may be measured separately. Due to the Ising symmetry, $\rho_+ = 1 - \rho_-$ so that an estimate of the coexistence curve consists of finding the densities of particle clusters alone. In the next chapter, we turn to the alternative method, which exploits systems subjected to two control parameters: the overall density $\overline{\rho}$ and temperature T. Determining a line of transitions, from disorder to order states, in the $\overline{\rho}$-T plane will serve as an estimate of the co-existence curve.

We construct the coexistence curves for six different SPBC with shifts $[H]$. Five of these system, with shifts of $H = \{0, 3, 4, 9, 18\}$, are relatively well behaved and will be discussed in this chapter and the next. The sixth system ($H = 6$)